International Journal of Refractory Metals & Hard Materials 82 (2019) 129–135

Contents lists available at ScienceDirect

International Journal of Refractory Metals & Hard Materials

journal homepage: www.elsevier.com/locate/IJRMHM

Microstructural, thermal and mechanical characterization of TiB_2–SiC composites doped with short carbon fibers

Sahar Nekahi[a], Farhad Sadegh Moghanlou[a], Mohammad Vajdi[a], Zohre Ahmadi[a], Amir Motallebzadeh[b], Mehdi Shahedi Asl[a,*]

[a] Department of Mechanical Engineering, University of Mohaghegh Ardabili, Ardabil, Iran
[b] Koc University Surface Science and Technology Center, Istanbul, Turkey

ARTICLE INFO

Keywords:
TiB_2–SiC
Carbon fiber
Spark plasma sintering
Microstructure
Thermal conductivity
Nanoindentation

ABSTRACT

Spark plasma sintering method, at the temperature of 1800 °C under the pressure of 40 MPa for 7 min, was employed for fabrication of TiB_2–SiC-based composites. The influences of short carbon fiber (C_f) addition (2 wt %) on microstructural, mechanical and thermal properties of TiB_2–SiC ceramics were studied. Carbon fiber addition increased the relative density of sintered composite which observed to have direct effect on mechanical and thermal properties. The mechanical properties of composites were measured by nanoindentation method. Hardness and elastic modulus of TiB_2/SiC interfaces in carbon fiber doped composite were measured 27.1 GPa and 445 GPa, respectively, while these values were obtained 24.2 GPa and 422 GPa for carbon-free sample. The thermal diffusivity of samples was measured by laser flash technique (LFT). It was found that TiB_2–SiC–C_f composite has a higher thermal conductivity (55 w/m.K) compared to TiB_2–SiC ceramic with a value of 54.8 w/m.K.

1. Introduction

Ultra high temperature ceramics (UHTCs) including carbides, borides and nitrides are a group of materials which have very high melting points and interesting capabilities to work at environments with high temperatures [1–7]. Among borides, titanium diboride (TiB_2) has been considered useful recently owing to a wide range of industrial application like wear resistance parts, refractory materials, cutting tools, cathodes for electrolysis in production of aluminum and electrodes for electro-discharge machining [8–11]. Special properties of TiB_2 are considerable hardness, excellent elastic modulus, good chemical stability, high thermal conductivity and low thermal expansion coefficient [12,13]. Nevertheless, monolithic TiB_2 has some limitations such as weak sinterability and low flexural strength [14]. Owing to the dominant covalent bonding of TiB_2, its sinterability is restricted, thus, a sintering temperature higher than 2000 °C is needed to achieve a full densification [15]. On the other hand, high temperatures cause fanatic grain growth and waste of energy which are not appropriate and lead to reduction in fracture toughness and flexural strength [16]. Hence, to lower the sintering temperature, several additives (carbon [17], carbide [18], silicide [19], and nitride [20,21] for instance) have been used as reinforcement or dopant in monolithic ceramics. Besides, these additives can reduce the oxide impurities that exist in the surface of TiB_2 powder and improve the mechanical properties [22–26].

Silicon carbide (SiC) as a common additive has special features such as high dimensional stability with great stiffness, low creep rate and low thermal expansion [27], which makes it a good candidate for applications that need dimensional stability at elevated temperatures. The amount of SiC added to TiB_2 matrix needs to be controlled since an appropriate content of this additive can enhance the high temperature oxidation resistance and mechanical properties [22,24,28]. The earlier methods of providing TiB_2–SiC composites (hot pressing or hot isostatic pressing) have some problems like low fracture toughness and high processing costs [18,29]. Later, reactive hot pressing has chosen as an alternative that provided better results than hot pressing [30]. However, in recent years, spark plasma sintering (SPS) has been used for fabricating ceramics and composites. The differences between SPS technique and other methods are relatively low temperature applied during densification as well as its short dwelling time [31–33]. ZrB_2, as another ultra-high temperature ceramic, has a similar behavior to TiB_2 and various studies have been conducted on the influence of adding SiC on ZrB_2-based composites. A progress in the mechanical and thermal properties and resistance against oxidation has been reported [34–48].

Carbon contains different morphologies (e.g. carbon nanotube,

* Corresponding author.
E-mail address: shahedi@uma.ac.ir (M. Shahedi Asl).

https://doi.org/10.1016/j.ijrmhm.2019.04.005
Received 23 March 2019; Received in revised form 3 April 2019; Accepted 9 April 2019
Available online 10 April 2019

graphite, graphene, carbon fiber, diamond, etc.) that can be added to composites and elevate their properties. Carbon additives promote the densification process by removing the impurities exist on the surface of starting powders [49–51]. Several papers have investigated the effect of adding carbon fiber [52,53], nanotube [54], graphene [55] or graphite [40,56] on mechanical properties of ZrB_2–SiC composites. Carbon fiber encompasses interesting advantages like thermodynamic adaptability, high-temperature forbearance, high tensile strength and stiffness and low weight [57,58]. Due to these features, carbon fiber got attention in aerospace and civil engineering. Yang et al. [53] manufactured fully dense ZrB_2–SiC composite by hot pressing and adding 20 vol% carbon fiber as a sintering aid. Taylor et al. [59] reported that the ZrB_2–SiC–C_f composite made by SPS exhibited a great critical thermal shock temperature as well as good thermal shock resistance.

Nevertheless, to the best of our knowledge, the influences of carbon fiber (C_f) addition on microstructural, thermal and mechanical features of TiB_2-based ceramics, reinforced with SiC, has not been available. In the present study, TiB_2–SiC composite doped with carbon fiber (2 wt% of the matrix) was manufactured by spark plasma sintering technique and its characteristics were compared with an undoped sample.

2. Experimental procedure

2.1. Materials and process

TiB_2 powders (size of particle 3–8 μm, purity > 99.9%, Xuzhou Hongwu Co., China), ultrafine SiC powders (size of 500 nm, purity > 99%, Xuzhou Hongwu Co., China) and carbon fibers (diameter of 5 μm, Torayca Sigmatex Ltd., United Kingdom) were purchased as starting materials. Carbon fibers (C_f) were manually cut in approximately 2 mm length. The raw materials were weighed in proper quantities based on the calculations: 13 g TiB_2 as matrix, 3.077 g SiC as reinforcement (25 vol% of matrix) and 0.26 g carbon fiber as dopant (2 wt% of matrix) only for the preparation of carbon-doped sample. At first, the chopped carbon fibers were dispersed in ethanol using an ultrasonic bath (WUC-D10H, Daihan, Korea) for half an hour. Then, the powders of TiB_2 plus submicron-sized SiC with the determined proportion were added to this suspension and homogenized again by 1 h extra ultrasonication. The mixture was heated on a magnetic stirrer for 4 h (MR 3001 k, Heidolph, Germany) next, it was dried inside an oven at the temperature of 120 °C for 20 h in order to evaporation of ethanol completely. The sintering of final mixture was carried out by spark plasma sintering apparatus (Nanozint 10i, Khalapoushan Felez Co., Iran). The prepared powder mixture were packed into a graphite die with a cylindrical shape and lined with pliable foils of graphite. The sample with a diameter of ~25 mm and the thickness of ~5 mm was sintered at 1800 °C for 7 min under the load of 40 MPa in vacuum. At the end, the furnace was cooled down to ambient temperature and the sample was taken from the die.

2.2. Characterizations

Archimedes method was applied for measuring the bulk density of sample and for determining the theoretical density, the rule of mixtures was used. The ratio of bulk density to theoretical density is called relative density. The surface of specimen was eliminated from the graphite contamination by grinding and polishing with diamond paste before characterizations. Phase analysis was fulfilled by the X-ray diffraction (D8 Advance, Bruker, Germany) analysis. The microstructure observations were performed by scanning electron microscope (Zeiss Ultra Plus, Carl Zeiss International, Germany). The size of grains was specified by an image analyzing software (ImageJ). HSC chemistry package (Outokumpu Research Oy, Finland) was employed to check the thermodynamic possibility of some reaction between components during the sintering. The thermal diffusivity was obtained by laser flash technique (LFA 467 HT HyperFlash, Netzsch, Germany). The standard samples with dimension of 1 × 1 cm^2 and thickness of 1 mm were prepared by wire-cut machining. In LFT method a laser energy pulse applies on one side of the sample and as a result of heat conduction, the temperature raise versus time is recorded at other side [60]. The thermal diffusion was calculated based on the temperature distribution and the time needed to reach a specified value. In order to calculate the thermal conductivity (k), the heat capacity (c) and density (ρ) of materials is needed. The thermal conductivity is calculated by the following relation where $\alpha$is thermal diffusivity:

$$k = \alpha\rho c \tag{1}$$

Nanoindentation method (Agilent G200, USA) with Berkovich diamond indenter tip was used for mechanical evaluations in which the geometry of tip was a three-sided pyramid and the applied load was ultra-low. At first, the penetration depth was noted and then the area of indent was assigned via the known geometry of the indentation tip. A load-displacement curve can be plotted simultaneously with indenting and estimate the contact area. Mechanical properties such as stiffness, Young modulus and hardness can be extracted from the curve. Oliver-Pharr technique, which recognizes the hardness based on area and depth, was chosen to determine the material properties. The maximum applied load was 400 mN at the fixed loading rate of 40 mN/s and holding time of 5 s. The hardness of material was calculated by Eq. (2) in which H is the hardness, P_{max} allocated to the maximum load and A_c represents the projected area of indentation.

$$H = \frac{P_{max}}{A_c} \tag{2}$$

Particular quantities from the load-displacement curve were elicited to identify the indent area by a software designed within the system according to Eq. (3) [61–65].

$$A_c = f(h_c) = 24.56 \times h_c^2 + 0.562 \times h_c + 0.003216 \tag{3}$$

where h_c is the contact depth based on Eq. (4), ε is given as a theoretical value of 0.75 for Berkovich indenter, S is stiffness and h_t represents the indenter displacement at maximum load.

$$h_c = h_t - \frac{\varepsilon}{S} \times P_{max} \tag{4}$$

Elastic modulus of material can be obtained using Eqs. (5)–(6), while E_s and E_i can be defined as elastic modulus of sample and indenter, also υ_s and υ_i are Poisson's coefficient of the indenter and sample, respectively.

$$S = \frac{dp}{dh} = \delta\frac{2}{\sqrt{\pi}}E_m\sqrt{A_c} \tag{5}$$

$$\frac{1}{E_m} = \frac{1-\upsilon_s^2}{E_s} + \frac{1-\upsilon_i^2}{E_i} \tag{6}$$

3. Results and discussion

The microstructure and phase analyses of the samples, sintered at the temperature of 1800 °C under the pressure of 40 MPa for 7 min, were performed by SEM and XRD, respectively. The addition of carbon fiber resulted in improved densification, because relative density values of 95.5% and 98.5% was estimated for TiB_2–SiC and TiB_2–SiC–C_f samples, respectively. Such outcome showed that adding small amount of C_f promoted the sinterability and increased the densification of TiB_2-based ceramic. It is proven that sintering temperature has significant role on densification of materials so that the higher sintering temperature, the better densification [66]. The effect of nitride additives such as Si_3N_4 on densification of TiB_2 reinforced with SiC composites was studied and a relative density of 99.8% was obtained for TiB_2–SiC–Si_3N_4 composite under SPS conditions of 1900 °C/7 min/40 MPa [9]. The influences of dwell time, applied pressure and temperature of ZrB_2–SiC–C_f composites using hot pressed method were

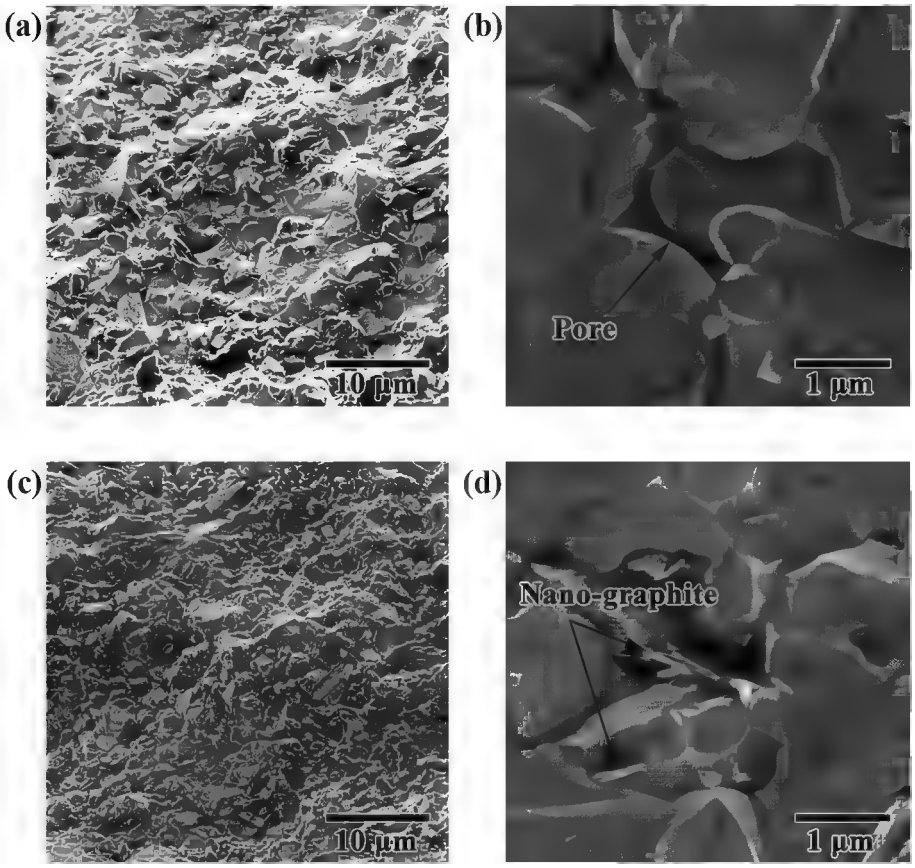

Fig. 1. SEM micrographs of fracture surface of (a,b) TiB_2–SiC and (c,d) TiB_2–SiC–C_f composites.

investigated and a fully dense composite was obtained by using 10 vol% carbon fiber and 20 vol% silicon carbide in ZrB_2 [67]. Since TiB_2 displays a densification behavior similar to ZrB_2, it is expected that adding carbon fiber to TiB_2–SiC composite can increase the relative density.

In order to get a better understanding of size and morphology of grains, SEM micrographs of fracture surfaces of TiB_2–SiC and TiB_2–SiC–C_f composites (Fig. 1) are needed. No obvious pore can be seen in the samples, especially in TiB_2–SiC–C_f composite with an approximate porosity content of 1.5%. Grains contain two fracture modes including transgranular (the grain itself fractures) and intergranular (fracture occurs in the grain boundaries). According to Fig. 1b, the multiplex fracture mode of grains can be seen, whereas the fracture mode of monolithic TiB_2 was reported to be transgranular [23]. Based on Fig. 1c, the sample with carbon fiber additive has smaller grains size. As shown in Fig. 1d, some new flaky phases with the thickness < 100 nm. Due to the detection of graphite by XRD (Fig. 2b), such flaky phases can be related to graphite. Closer look at Fig. 1d, reveals two nano-flakes of graphite (thickness $<$ 50 nm) in this fractograph.

The X-ray diffraction analyses of TiB_2–SiC and TiB_2–SiC–C_f composites are shown in Fig. 2a–b, respectively. The phases of TiB_2 and SiC as the main starting powders are identified in both samples. Trace of graphite is detected in TiB_2–SiC–C_f composite (Fig. 2b), due to the crystalline structure of carbon fiber in the form of graphite. The intensities of TiB_2 and SiC peaks show no obvious differences with adding C_f as dopant. According to XRD patterns of the starting powders (not shown here), the existence of oxide impurities such as TiO_2 and B_2O_3 on the external surface of TiB_2, and also SiO_2 on the surface of SiC can be confirmed.

During the sintering process, SiC may react with such impurities (TiO_2 and B_2O_3) according to Eqs. (7) and (8) which cause the formation of TiC, B_4C and SiO_2.

$$TiO_2 + SiC = TiC + SiO_2 \quad (7)$$

$$4B_2O_3(g) + 7SiC = 2B_4C + 7SiO(g) + 5CO(g) \quad (8)$$

As shown in Fig. 3, the reaction of Eq. (7) is possible at any temperature and the reaction of Eq. (8) is thermodynamically favorable at the temperatures over 1866 °C and standard atmospheric pressure (1 atm). Although the sintering sample experienced the maximum temperature of 1800 °C, the reaction of Eq. (8) seems to be possible under vacuum conditions. Considering that the process of sintering occurs in vacuum, the gaseous phases (produced via Eq. (8)) escape from the sintered samples.

On the other hand, because of the presence of carbon fiber in TiB_2–SiC–C_f specimen, it is possible for carbon to react with TiO_2, B_2O_3 and SiO_2 to form TiC, B_4C and SiC phases in accord with Eqs. (9)–(11):

$$TiO_2 + 3C = TiC + 2CO(g) \quad (9)$$

$$2B_2O_3 + 7C = B_4C + 6CO(g) \quad (10)$$

$$SiO_2 + 3C = SiC + 2CO(g) \quad (11)$$

Reactions based on Eqs. (9)–(11) are also thermodynamically feasible at temperatures over 1288 °C, 1567 °C and 1522 °C, respectively (Fig. 4).

Based on SEM results of the polished surfaces of TiB_2–SiC (Figs. 3a–b) and TiB_2–SiC–C_f (Fig. 3c–d) composites, the reduction in porosity content of the sample doped with carbon fiber is tangible, hence, the relative density of such sample can be expected to be higher. This statement is consistent with the obtained values of 95.5% and 98.5% for the relative density of TiB_2–SiC and TiB_2–SiC–C_f specimens, respectively. It can be seen from the images that the amount of rounded black spots, which shows porosities, is much higher in TiB_2–SiC composite in comparison with the other one. Therefore, it can be concluded that carbon fiber additive has reduced the porosity and made the piece

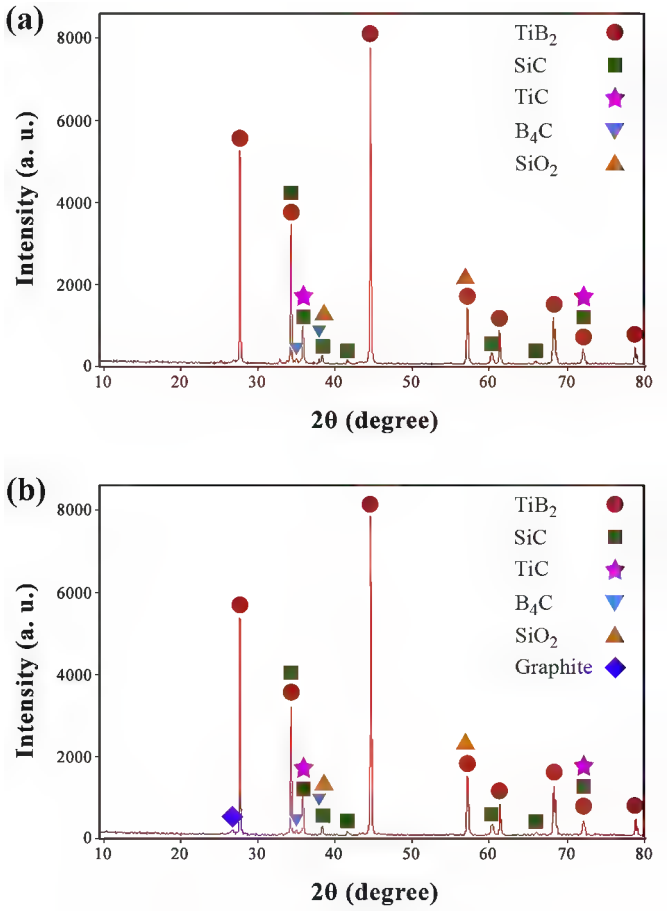

Fig. 2. XRD patterns of (a) carbon-free and (b) carbon-doped TiB_2–SiC composites.

to be denser. Regarding the high-magnification SEM image of TiB_2–SiC ceramic, shown in Fig. 5b, the most visible area is a light-gray background and due to the higher content of TiB_2 in the mixture, it can be related to TiB_2. In addition, the dark-gray regions are most likely to be SiC particles because they contain less volume fraction of phases. Besides, Fig. 5a presents that the dark SiC reinforcements have distributed uniformly in the TiB_2 matrix and it seems that the phases of TiB_2 and SiC mixed together in an acceptable manner.

Some needle-like morphology of carbon fiber with black color are observable in the SEM micrograph of Fig. 5c in which the middle part of the phases is completely black and the round of carbon fiber (black parts) is grayed out. More precisely, it appears that one of these carbon fibers has fully changed its color and become gray which may be due to a reaction. As shown in the high-magnification SEM image of TiB_2–SiC–C_f sample (Fig. 5d), the black region is part of graphite which has been remained unreacted. The XRD patterns also confirm the existence of graphite phase, however, the margins of this carbon fiber has reacted with adjacent grains and converted to other phases. Since the reactions start from the surface and then progress to the center, it seems that there was not enough time or temperature for the central part of this fiber to participate in the reaction. Apparently, the color of new formed phase created around the C_f is extremely similar to that of SiC, thus, according to Eq. (11), the formation of SiC through the reduction of SiO_2 may be possible. Since the amounts of in-situ formed phases such as TiC and B_4C were low, it was difficult to detect them by SEM.

The nanoindentation technique was used to determine the mechanical properties of TiB_2–SiC and TiB_2–SiC–C_f samples and the obtained results are given in Tables 1–2. Analyzing the properties such as hardness, stiffness and elastic modulus is one of the applications of this method. Based on Table 1, the value of hardness at TiB_2/SiC interface is 24.2 GPa whereas the hardness of TiB_2 grain is 33.8 GPa. It appears that the striking decrease in the hardness of at the interfaces is related to the lower hardness of SiC than TiB_2 matrix. A similar trend can be seen in Table 2, but, it should be noted that the hardness values of both TiB_2 grains and TiB_2/SiC interfaces in TiB_2–SiC–C_f composite are higher than those measured for TiB_2–SiC ceramic. Such a comparison is attributed to the higher relative density of carbon-doped sample. The elastic modulus of 516 GPa for TiB_2 grain in TiB_2–SiC–C_f composite (Table 2) is near to that measured for TiB_2 (523 GPa) in TiB_2–SiC sample (Table 1). Elastic modulus is susceptible to porosity and increases with reduction in the porosity content. Hence, a remarkable enhancement in the elastic modulus value at TiB_2/SiC interface from 422 in TiB_2–SiC ceramic to

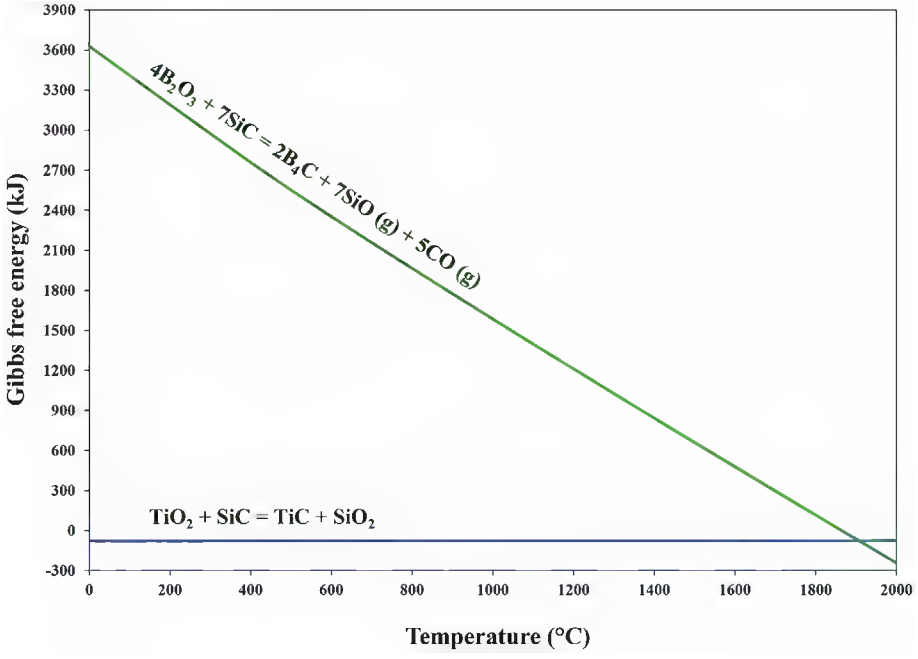

Fig. 3. Standard Gibbs free energy versus temperature for the chemical reactions of Eqs. (7)–(8).

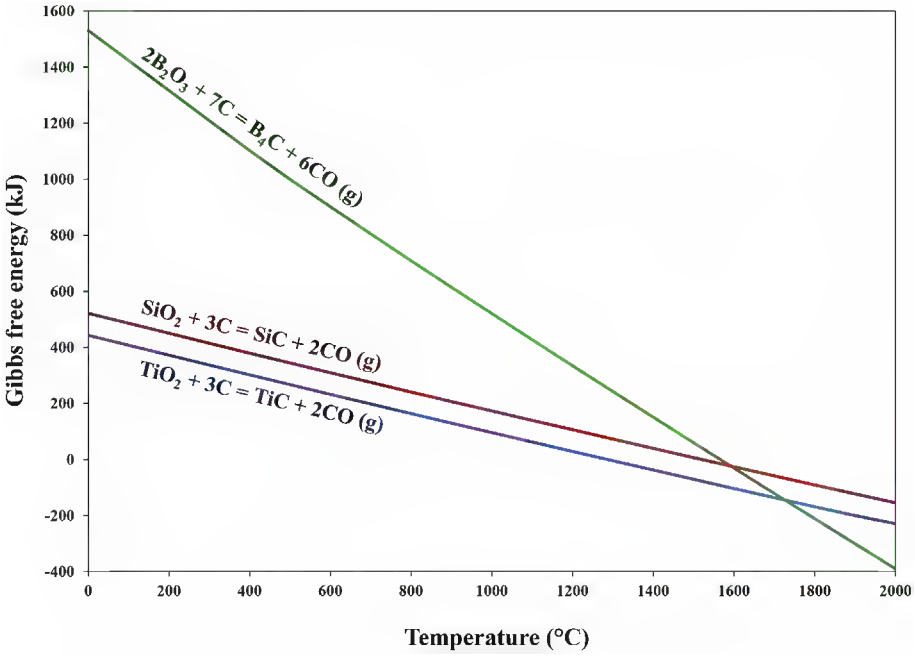

Fig. 4. Standard Gibbs free energy versus temperature for the chemical reactions of Eqs. (9)–(11).

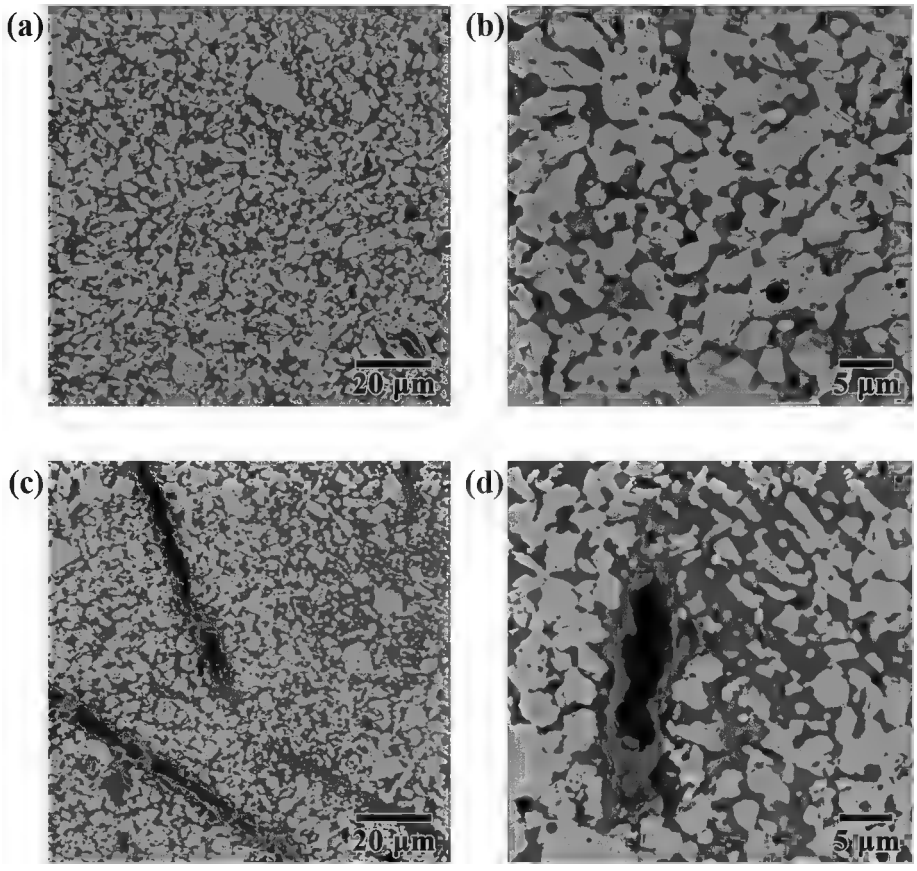

Fig. 5. SEM images of polished surface of (a,b) TiB_2–SiC and (c,d) TiB_2–SiC–C_f composites.

445 GPa in TiB_2–SiC–C_f composite can be related to the positive role of carbon fiber additive on densification improvement.

The thermal diffusivity of samples was obtained by laser flash technique. The heat capacity values were calculated by rule of mixture method and using the measured bulk densities. The thermal conductivity of samples was calculated by Eq. (1). The thermal conductivities of 54.83 w/m.K and 54.98 w/m.K were obtained for TiB_2–SiC and TiB_2–SiC–C_f composites, respectively. As it is obvious, the thermal conductivity of TiB_2–SiC–C_f sample has higher value than TiB_2–SiC ceramic. More porosity of TiB_2–SiC ceramic has negative effect on thermal conductivity, since porosities filled with gas and have conductivities in order of 0.01 w/m.K as an insulator. On the other

Table 1
Mechanical properties of TiB_2 grains and TiB_2/SiC interfaces in TiB_2–SiC ceramic.

	Elastic modulus (GPa)	Hardness (GPa)	Stiffness (MN/m)
TiB_2 grain	523	33.8	1.43
TiB_2/SiC interface	422	24.2	1.52

Table 2
Mechanical properties of TiB_2 grains and TiB_2/SiC interfaces in TiB_2–SiC–C_f composite.

	Elastic modulus (GPa)	Hardness (GPa)	Stiffness (MN/m)
TiB_2 grain	516	36.5	1.39
TiB_2/SiC interface	445	27.1	1.46

hand, based on Eq. (1), the density and heat capacity of materials play direct role in thermal conductivity value. On one hand, the TiB_2–SiC composite has lower density and on the other hand its specific heat capacity is lower than TiB_2–SiC–C_f sample. It can be concluded that the positive and negative effects of mentioned parameters caused inconsiderable enhancement on thermal conductivity of TiB_2–SiC composite by adding carbon fibers.

4. Conclusions

SiC reinforced TiB_2 matrix composites, doped with carbon fiber, was fabricated by spark plasma sintering method. The effect of carbon fiber addition on microstructural, thermal and mechanical properties of TiB_2–SiC composite were investigated. Results showed a better densification in TiB_2–SiC–C_f sample with enhanced mechanical properties. Thermal diffusivity was obtained via laser flash technique and used to calculate the thermal conductivity. The results demonstrated that adding carbon fiber increased the thermal conductivity of base composite.

References

[1] M. Shahedi Asl, B. Nayebi, Z. Ahmadi, M. Jaberi Zamharir, M. Shokouhimehr, Effects of carbon additives on the properties of ZrB2–based composites: a review, Ceram. Int. 44 (2018) 7334–7348, https://doi.org/10.1016/j.ceramint.2018.01.214.

[2] Y. Azizian-Kalandaragh, A.S. Namini, Z. Ahmadi, M. Shahedi Asl, Reinforcing effects of SiC whiskers and carbon nanoparticles in spark plasma sintered ZrB2 matrix composites, Ceram. Int. 44 (2018) 19932–19938, https://doi.org/10.1016/j.ceramint.2018.07.258.

[3] A. Babapoor, M.S. Asl, Z. Ahmadi, A.S. Namini, Effects of spark plasma sintering temperature on densification, hardness and thermal conductivity of titanium carbide, Ceram. Int. 44 (2018) 14541–14546, https://doi.org/10.1016/j.ceramint.2018.05.071.

[4] A. Sabahi Namini, Z. Ahmadi, A. Babapoor, M. Shokouhimehr, M. Shahedi Asl, Microstructure and thermomechanical characteristics of spark plasma sintered TiC ceramics doped with nano-sized WC, Ceram. Int. 45 (2019) 2153–2160, https://doi.org/10.1016/j.ceramint.2018.10.125.

[5] S.A. Delbari, B. Nayebi, E. Ghasali, M. Shokouhimehr, M. Shahedi Asl, Spark plasma sintering of TiN ceramics codoped with SiC and CNT, Ceram. Int. 45 (2019) 3207–3216, https://doi.org/10.1016/j.ceramint.2018.10.223.

[6] M. Shahedi Asl, M. Ghassemi Kakroudi, F. Golestani-Fard, H. Nasiri, A Taguchi approach to the influence of hot pressing parameters and SiC content on the sinterability of ZrB2-based composites, Int. J. Refract. Met. Hard Mater. 51 (2015) 81–90, https://doi.org/10.1016/j.ijrmhm.2015.03.002.

[7] M. Shahedi Asl, M. Ghassemi Kakroudi, M. Rezvani, F. Golestani-Fard, Significance of hot pressing parameters on the microstructure and densification behavior of zirconium diboride, Int. J. Refract. Met. Hard Mater. 50 (2015) 140–145, https://doi.org/10.1016/j.ijrmhm.2015.01.004.

[8] Z. Hamidzadeh Mahaseni, M. Dashti Germi, Z. Ahmadi, M. Shahedi Asl, Microstructural investigation of spark plasma sintered TiB2 ceramics with Si3N4 addition, Ceram. Int. 44 (2018) 13367–13372, https://doi.org/10.1016/j.ceramint.2018.04.171.

[9] M. Dashti Germi, Z. Hamidzadeh Mahaseni, Z. Ahmadi, M. Shahedi Asl, Phase evolution during spark plasma sintering of novel Si3N4-doped TiB2–SiC composite, Mater. Charact. 145 (2018) 225–232, https://doi.org/10.1016/j.matchar.2018.08.043.

[10] M. Shahedi Asl, S.A. Delbari, F. Shayesteh, Z. Ahmadi, A. Motallebzadeh, Reactive spark plasma sintering of TiB2–SiC–TiN novel composite, Int. J. Refract. Met. Hard Mater. 81 (2019) 119–126, https://doi.org/10.1016/j.ijrmhm.2019.02.022.

[11] F. Shayesteh, S.A. Delbari, Z. Ahmadi, M. Shokouhimehr, M. Shahedi Asl, Influence of TiN dopant on microstructure of TiB2 ceramic sintered by spark plasma, Ceram. Int. 45 (2019) 5306–5311, https://doi.org/10.1016/j.ceramint.2018.11.228.

[12] G.B. Raju, B. Basu, Development of high temperature TiB2-based ceramics, Key Eng. Mater. 395 (2009) 89–124, https://doi.org/10.4028/www.scientific.net/KEM.395.89.

[13] T.S.R.Ch. Murthy, J.K. Sonber, K. Sairam, R.D. Bedse, J.K. Chakarvartty, Development of refractory and rare earth metal borides & carbides for high temperature applications, Mater. Today Proc. 3 (2016) 3104–3113, https://doi.org/10.1016/j.matpr.2016.09.026.

[14] J.-H. Park, Y.-H. Lee, Y.-H. Koh, H.-E. Kim, S. Su Baek, Effect of hot-pressing temperature on densification and mechanical properties of titanium diboride with silicon nitride as a sintering aid, J. Am. Ceram. Soc. 83 (2004) 1542–1544, https://doi.org/10.1111/j.1151-2916.2000.tb01428.x.

[15] M. Barandika, J. Sánchez, T. Rojo, R. Cortés, F. Castro, Fe-Ni-Ti binder phases for TiB2-based cermets: a thermodynamic approach, Scr. Mater. 39 (1998) 1395–1400, https://doi.org/10.1016/S1359-6462(98)00312-1.

[16] S.K. Bhaumik, C. Divakar, A.K. Singh, G.S. Upadhyaya, Synthesis and sintering of TiB2 and TiB2–TiC composite under high pressure, Mater. Sci. Eng. A 279 (2000) 275–281, https://doi.org/10.1016/S0921-5093(99)00217-8.

[17] M.S. Jensen, M.-A. Einarsrud, T. Grande, The effect of surface oxides during hot pressing of TiB2, J. Am. Ceram. Soc. 92 (2009) 623–630, https://doi.org/10.1111/j.1551-2916.2009.02923.x.

[18] S. Torizuka, K. Sato, H. Nishio, T. Kishi, Effect of SiC on interfacial reaction and sintering mechanism of TiB2, J. Am. Ceram. Soc. 78 (1995) 1606–1610, https://doi.org/10.1111/j.1151-2916.1995.tb08858.x.

[19] D. Jain, K.M. Reddy, A. Mukhopadhyay, B. Basu, Achieving uniform microstructure and superior mechanical properties in ultrafine grained TiB2–TiSi2 composites using innovative multi stage spark plasma sintering, Mater. Sci. Eng. A 528 (2010) 200–207, https://doi.org/10.1016/j.msea.2010.09.022.

[20] L.-H. Li, H.-E. Kim, E. Son Kang, Sintering and mechanical properties of titanium diboride with aluminum nitride as a sintering aid, J. Eur. Ceram. Soc. 22 (2002) 973–977, https://doi.org/10.1016/S0955-2219(01)00403-4.

[21] J.-H. Park, Y.-H. Koh, H.-E. Kim, C.S. Hwang, E.S. Kang, Densification and mechanical properties of titanium diboride with silicon nitride as a sintering aid, J. Am. Ceram. Soc. 82 (2004) 3037–3042, https://doi.org/10.1111/j.1151-2916.1999.tb02199.x.

[22] K. Farhadi, A. Sabahi Namini, M. Shahedi Asl, A. Mohammadzadeh, M. Ghassemi Kakroudi, Characterization of hot pressed SiC whisker reinforced TiB2 based composites, Int. J. Refract. Met. Hard Mater. 61 (2016) 84–90, https://doi.org/10.1016/j.ijrmhm.2016.08.004.

[23] A. Sabahi Namini, S.N. Seyed Gogani, M. Shahedi Asl, K. Farhadi, M. Ghassemi Kakroudi, A. Mohammadzadeh, Microstructural development and mechanical properties of hot pressed SiC reinforced TiB2 based composite, Int. J. Refract. Met. Hard Mater. 51 (2015) 169–179, https://doi.org/10.1016/j.ijrmhm.2015.03.014.

[24] M. Shahedi Asl, Z. Ahmadi, S. Parvizi, Z. Balak, I. Farahbakhsh, Contribution of SiC particle size and spark plasma sintering conditions on grain growth and hardness of TiB2 composites, Ceram. Int. 43 (2017) 13924–13931, https://doi.org/10.1016/j.ceramint.2017.07.121.

[25] Z. Ahmadi, B. Nayebi, M. Shahedi Asl, I. Farahbakhsh, Z. Balak, Densification improvement of spark plasma sintered TiB2-based composites with micron-, submicron- and nano-sized SiC particulates, Ceram. Int. 44 (2018) 11431–11437, https://doi.org/10.1016/j.ceramint.2018.03.202.

[26] M. Shahedi Asl, M. Ghassemi Kakroudi, B. Nayebi, H. Nasiri, Taguchi analysis on the effect of hot pressing parameters on density and hardness of zirconium diboride, Int. J. Refract. Met. Hard Mater. 50 (2015) 313–320, https://doi.org/10.1016/j.ijrmhm.2014.09.006.

[27] L.L. Snead, T. Nozawa, Y. Katoh, T.-S. Byun, S. Kondo, D.A. Petti, Handbook of SiC properties for fuel performance modeling, J. Nucl. Mater. 371 (2007) 329–377, https://doi.org/10.1016/j.jnucmat.2007.05.016.

[28] M. Shahedi Asl, A. Sabahi Namini, M. Ghassemi Kakroudi, Influence of silicon carbide addition on the microstructural development of hot pressed zirconium and titanium diborides, Ceram. Int. 42 (2016) 5375–5381, https://doi.org/10.1016/j.ceramint.2015.12.072.

[29] S. Baik, P.F. Becher, Effect of pxygen contamination on densification of TiB2, J. Am. Ceram. Soc. 70 (1987) 527–530, https://doi.org/10.1111/j.1151-2916.1987.tb05699.x.

[30] G. Zhao, C. Huang, H. Liu, B. Zou, H. Zhu, J. Wang, A study on in-situ synthesis of TiB2–SiC ceramic composites by reactive hot pressing, Ceram. Int. 40 (2014) 2305–2313, https://doi.org/10.1016/j.ceramint.2013.07.152.

[31] A. Sabahi Namini, M. Azadbeh, M. Shahedi Asl, Effects of in-situ formed TiB whiskers on microstructure and mechanical properties of spark plasma sintered Ti–B4C and Ti–TiB2 composites, Sci. Iran. 25 (2018) 762–771, https://doi.org/10.24200/sci.2017.4499.

[32] M. Akhlaghi, S.A. Tayebifard, E. Salahi, M. Shahedi Asl, Spark plasma sintering of TiAl–Ti3AlC2 composite, Ceram. Int. 44 (2018) 21759–21764, https://doi.org/10.1016/j.ceramint.2018.08.272.

[33] Z.A. Munir, U. Anselmi-Tamburini, M. Ohyanagi, The effect of electric field and pressure on the synthesis and consolidation of materials: a review of the spark plasma sintering method, J. Mater. Sci. 41 (2006) 763–777, https://doi.org/10.1007/s10853-006-6555-2.

[34] M. Shahedi Asl, B. Nayebi, Z. Ahmadi, P. Pirmohammadi, M. Ghassemi Kakroudi, Fractographical characterization of hot pressed and pressureless sintered SiAlON-

doped ZrB2–SiC composites, Mater. Charact. 102 (2015) 137–145, https://doi.org/10.1016/j.matchar.2015.03.002.
[35] Z. Ahmadi, B. Nayebi, M. Shahedi Asl, M. Ghassemi Kakroudi, I. Farahbakhsh, Sintering behavior of ZrB2–SiC composites doped with Si3N4: a fractographical approach, Ceram. Int. 43 (2017) 9699–9708, https://doi.org/10.1016/j.ceramint.2017.04.144.
[36] B. Mohammadpour, Z. Ahmadi, M. Shokouhimehr, M. Shahedi Asl, Spark plasma sintering of Al-doped ZrB2–SiC composite, Ceram. Int. 45 (2019) 4262–4267, https://doi.org/10.1016/j.ceramint.2018.11.098.
[37] M. Shahedi Asl, B. Nayebi, M. Shokouhimehr, TEM characterization of spark plasma sintered ZrB2–SiC–graphene nanocomposite, Ceram. Int. 44 (2018) 15269–15273, https://doi.org/10.1016/j.ceramint.2018.05.170.
[38] S. Parvizi, Z. Ahmadi, M.J. Zamharir, M. Shahedi Asl, Synergistic effects of graphite nano-flakes and submicron SiC particles on the characteristics of spark plasma sintered ZrB2 nanocomposites, Int. J. Refract. Met. Hard Mater. 75 (2018) 10–17, https://doi.org/10.1016/j.ijrmhm.2018.03.017.
[39] M. Shahedi Asl, B. Nayebi, Z. Ahmadi, S. Parvizi, M. Shokouhimehr, A novel ZrB2–VB2–ZrC composite fabricated by reactive spark plasma sintering, Mater. Sci. Eng. A 731 (2018) 131–139, https://doi.org/10.1016/j.msea.2018.06.008.
[40] M. Shahedi Asl, M. Ghassemi Kakroudi, R. Abedi Kondolaji, H. Nasiri, Influence of graphite nano-flakes on densification and mechanical properties of hot-pressed ZrB2–SiC composite, Ceram. Int. 41 (2015) 5843–5851, https://doi.org/10.1016/j.ceramint.2015.01.014.
[41] Z. Ahmadi, B. Nayebi, M. Shahedi Asl, M. Ghassemi Kakroudi, Fractographical characterization of hot pressed and pressureless sintered AlN-doped ZrB2–SiC composites, Mater. Charact. 110 (2015) 77–85, https://doi.org/10.1016/j.matchar.2015.10.016.
[42] I. Farahbakhsh, Z. Ahmadi, M. Shahedi Asl, Densification, microstructure and mechanical properties of hot pressed ZrB2–SiC ceramic doped with nano-sized carbon black, Ceram. Int. 43 (2017) 8411–8417, https://doi.org/10.1016/j.ceramint.2017.03.188.
[43] E. Ghasali, M. Shahedi Asl, Microstructural development during spark plasma sintering of ZrB2–SiC–Ti composite, Ceram. Int. 44 (2018) 18078–18083, https://doi.org/10.1016/j.ceramint.2018.07.011.
[44] M. Shahedi Asl, A statistical approach towards processing optimization of ZrB2–SiC–graphite nanocomposites. Part I: relative density, Ceram. Int. 44 (2018) 6935–6939, https://doi.org/10.1016/j.ceramint.2018.01.122.
[45] M. Shahedi Asl, M. Ghassemi Kakroudi, A processing-microstructure correlation in ZrB2–SiC composites hot-pressed under a load of 10 MPa, Univers, J. Mater. Sci. 3 (2015) 14–21, https://doi.org/10.13189/ujms.2015.030103.
[46] M. Mallik, S. Roy, K.K. Ray, R. Mitra, Effect of SiC content, additives and process parameters on densification and structure–property relations of pressureless sintered ZrB2–SiC composites, Ceram. Int. 39 (2013) 2915–2932, https://doi.org/10.1016/j.ceramint.2012.09.066.
[47] E. Zapata-Solvas, D.D. Jayaseelan, H.T. Lin, P. Brown, W.E. Lee, Mechanical properties of ZrB2- and HfB2-based ultra-high temperature ceramics fabricated by spark plasma sintering, J. Eur. Ceram. Soc. 33 (2013) 1373–1386, https://doi.org/10.1016/j.jeurceramsoc.2012.12.009.
[48] N. Pourmohammadie Vafa, M. Shahedi Asl, M. Jaberi Zamharir, M. Ghassemi Kakroudi, Reactive hot pressing of ZrB2-based composites with changes in ZrO2/SiC ratio and sintering conditions. Part I: densification behavior, Ceram. Int. 41 (2015) 8388–8396, https://doi.org/10.1016/j.ceramint.2015.03.033.
[49] M. Khoeini, A. Nemati, M. Zakeri, M. Shahedi Asl, Pressureless sintering of ZrB2 ceramics codoped with TiC and graphite, Int. J. Refract. Met. Hard Mater. 81 (2019) 189–195, https://doi.org/10.1016/j.ijrmhm.2019.02.026.
[50] M. Khoeini, A. Nemati, M. Zakeri, M. Tamizifar, H. Samadi, Comprehensive study on the effect of SiC and carbon additives on the pressureless sintering and microstructural and mechanical characteristics of new ultra-high temperature ZrB2 ceramics, Ceram. Int. 41 (2015) 11456–11463, https://doi.org/10.1016/j.ceramint.2015.05.110.
[51] Z. Balak, M. Zakeri, M. Rahimipour, E. Salahi, Taguchi design and hardness optimization of ZrB 2 -based composites reinforced with chopped carbon fiber and different additives and prepared by SPS, J. Alloys Compd. 639 (2015) 617–625, https://doi.org/10.1016/j.jallcom.2015.03.131.
[52] M. Shahedi Asl, Microstructure, hardness and fracture toughness of spark plasma sintered ZrB2–SiC–Cf composites, Ceram. Int. 43 (2017) 15047–15052, https://doi.org/10.1016/j.ceramint.2017.08.030.
[53] P. Zhang, P. Hu, X. Zhang, J. Han, S. Meng, Processing and characterization of ZrB2–SiCW ultra-high temperature ceramics, J. Alloys Compd. 472 (2009) 358–362, https://doi.org/10.1016/j.jallcom.2008.04.082.
[54] M. Shahedi Asl, I. Farahbakhsh, B. Nayebi, Characteristics of multi-walled carbon nanotube toughened ZrB2–SiC ceramic composite prepared by hot pressing, Ceram. Int. 42 (2016) 1950–1958, https://doi.org/10.1016/j.ceramint.2015.09.165.
[55] M. Shahedi Asl, M. Ghassemi Kakroudi, Characterization of hot-pressed graphene reinforced ZrB2–SiC composite, Mater. Sci. Eng. A 625 (2015) 385–392, https://doi.org/10.1016/j.msea.2014.12.028.
[56] M. Shahedi Asl, M.J. Zamharir, Z. Ahmadi, S. Parvizi, Effects of nano-graphite content on the characteristics of spark plasma sintered ZrB2–SiC composites, Mater. Sci. Eng. A 716 (2018) 99–106, https://doi.org/10.1016/j.msea.2018.01.038.
[57] J. Liu, Z. Yue, H. Fong, Continuous nanoscale carbon fibers with superior mechanical strength, Small. 5 (2009) 536–542, https://doi.org/10.1002/smll.200801440.
[58] R.E. Tressler, Recent developments in fibers and interphases for high temperature ceramic matrix composites, Compos. Part A Appl. Sci. Manuf. 30 (1999) 429–437, https://doi.org/10.1016/S1359-835X(98)00131-6.
[59] D. Taylor, P. Cornetti, N. Pugno, The fracture mechanics of finite crack extension, Eng. Fract. Mech. 72 (2005) 1021–1038, https://doi.org/10.1016/j.engfracmech.2004.07.001.
[60] M. Vajdi, F. Sadegh Moghanlou, Z. Ahmadi, A. Motallebzadeh, M. Shahedi Asl, Thermal diffusivity and microstructure of spark plasma sintered TiB2SiC Ti composite, Ceram. Int. 45 (2019) 8333–8344, https://doi.org/10.1016/j.ceramint.2019.01.141.
[61] A. Sabahi Namini, A. Motallebzadeh, B. Nayebi, M. Shahedi Asl, M. Azadbeh, Microstructure–mechanical properties correlation in spark plasma sintered Ti–4.8 wt.% TiB2 composites, Mater. Chem. Phys. 223 (2019) 789–796, https://doi.org/10.1016/j.matchemphys.2018.11.057.
[62] E. Broitman, Indentation hardness measurements at macro-, micro-, and nanoscale: a critical overview, Tribol. Lett. 65 (2017) 23, , https://doi.org/10.1007/s11249-016-0805-5.
[63] B. Poon, D. Rittel, G. Ravichandran, An analysis of nanoindentation in linearly elastic solids, Int. J. Solids Struct. 45 (2008) 6018–6033, https://doi.org/10.1016/j.ijsolstr.2008.07.021.
[64] W.C. Oliver, G.M. Pharr, Measurement of hardness and elastic modulus by instrumented indentation: advances in understanding and refinements to methodology, J. Mater. Res. 19 (2004) 3–20, https://doi.org/10.1557/jmr.2004.19.1.3.
[65] Q. Kan, W. Yan, G. Kang, Q. Sun, Oliver–Pharr indentation method in determining elastic moduli of shape memory alloys—a phase transformable material, J. Mech. Phys. Solids. 61 (2013) 2015–2033, https://doi.org/10.1016/j.jmps.2013.05.007.
[66] J. Lin, Y. Yang, H. Zhang, J. Gong, Effects of CNTs content on the microstructure and mechanical properties of spark plasma sintered TiB2-SiC ceramics, Ceram. Int. 43 (2017) 1284–1289, https://doi.org/10.1016/j.ceramint.2016.10.078.
[67] M. Shahedi Asl, F. Golmohammadi, M. Ghassemi Kakroudi, M. Shokouhimehr, Synergetic effects of SiC and Csf in ZrB2-based ceramic composites. Part I: densification behavior, Ceram. Int. 42 (2016) 4498–4506, https://doi.org/10.1016/j.ceramint.2015.11.139.